RSC Advances

PAPER

View Article Online
View Journal | View Issue

Cite this: *RSC Adv.*, 2019, **9**, 29097

TiO_2–Au composite nanofibers for photocatalytic hydrogen evolution

Xiaojiao Yang,[a] Xuelian Wu,[b] Jun Li[a] and Ying Liu *[a]

TiO_2-based materials for photocatalytic hydrogen (H_2) evolution have attracted much interest as a renewable approach for clean energy applications. TiO_2–Au composite nanofibers (NFs) with an average fiber diameter of ~160 nm have been fabricated by electrospinning combined with calcination treatment. *In situ* reduced gold nanoparticles (NPs) with uniform size (~10 nm) are found to disperse homogenously in the TiO_2 NF matrix. The TiO_2–Au composite NFs catalyst can significantly enhance the photocatalytic H_2 generation with an extremely high rate of 12 440 μmol g^{-1} h^{-1}, corresponding to an adequate apparent quantum yield of 5.11% at 400 nm, which is 25 times and 10 times those of P25 (584 μmol g^{-1} h^{-1}) and pure TiO_2 NFs (1254 μmol g^{-1} h^{-1}), respectively. Furthermore, detailed studies indicate that the H_2 evolution efficiency of the TiO_2–Au composite NF catalyst is highly dependent on the gold content. This work provides a strategy to develop highly efficient catalysts for H_2 evolution.

Received 5th July 2019
Accepted 9th September 2019

DOI: 10.1039/c9ra05113a

rsc.li/rsc-advances

Introduction

Photocatalytic hydrogen (H_2) evolution has drawn great attention as a promising approach to overcome the energy crisis by converting solar energy to H_2 fuel directly.[1–3] On the basis of Fujishima's pioneering work,[4] numerous semiconductor-based photocatalysts have been developed to produce H_2 (such as TiO_2,[5] CdS,[6] ZnO,[7] Cu_2O,[8] *etc.*). TiO_2 has attracted much attention owing to its excellent properties including low cost, environmental friendliness, strong oxidizing power and high stability.[9] However, the photocatalytic efficiency of TiO_2-based materials is still limited, with a low solar light harvesting capability due to its wide band gap and high charge recombination rate.[10] Therefore, it is important to develop TiO_2-based photocatalysts for increasing the light harvesting and promoting the photoinduced charge separation during the H_2 generation process.

Numerous attempts have been devoted to improving the H_2 generation efficiency of TiO_2 materials including doping,[11] metal deposition,[10,12] and heterostructures formation.[13] Chiu[14] has designed a quaternary Ti–Nb–Ta–Zr–O mixed-oxide nanotube arrays; Hsieh[15] has conducted compact deposition of In_2S_3 nanocrystals on the TiO_2 nanowire array; Li[16] has prepared by electrodepositing a Cu_2O layer on the surface of Au particle-coated TiO_2 arrays; Chang[17] has synthesized CdS/CdSe co-sensitized brookite TiO_2 nanostructures with hydrogen doping (H:TiO_2/CdS/CdSe) in a facile solution reaction. All these TiO_2-based materials were developed to enhance the amount of accessible charge carriers, modify the electronic structure, improve the hole injection kinetics for the photoelectrochemical water splitting.

Combining TiO_2 with highly dispersed noble metal nanoparticles (NPs) as cocatalyst is a feasible approach for enhancing the photocatalytic performance.[18] Among the noble metal NPs (*i.e.* Au,[19,20] Ag,[21] Pt,[22] Pd[23,24]), gold with finite NPs size can spatially separate the photogenerated charge carriers.[3,25] Much efforts have been focused on TiO_2 NPs as matrix and different size or shape of gold NPs, to understand the fine-tuning the surface plasmon resonance effect.[26] Pu and his colleagues[27] have reported that the photocatalytic ability of TiO_2 nanowires can be effectively enhanced in the entire UV-visible region by adopting different shapes of the decorated Au nanostructures. Compared to other nanostructures, TiO_2 nanofibers (NFs) possess additional advantages due to its specific morphologies with large aspect ratio and large specific surface area for photocatalytic activity.[28] Yoshikawa[29] has proved that the TiO_2 NFs catalyst can promote the opportunities for photocatalytic H_2 evolution. Xia and Li[30,31] successfully fabricated the TiO_2 NFs and its composite deposited with gold NPs. However, there are seldom literatures studying the TiO_2–Au composite NFs as photocatalyst for H_2 generation and the effect of gold content on photocatalytic performance.

Herein, TiO_2–Au NFs composites with different gold content were fabricated *via* electrospinning combined with subsequent calcination. The gold NPs are *in situ* reduced during the calcination process while the polymer components are decomposed and removed to form TiO_2 NFs.[32] The gold content is tuned by controlling the amount of gold precursor added during

[a]*College of Materials Science and Engineering, Sichuan University, No. 24 South Section 1, Yihuan Road, Chengdu 610065, P. R. China. E-mail: liuying5536@scu.edu.cn*

[b]*International Collaborative Laboratory of 2D Materials for Optoelectronics Science and Technology of MOE, Institute of Microscale Optoelectronics, Shenzhen University, Shenzhen 518060, China*

synthesis process, and all the chemicals are mixed homogenously in solution with molecular level. The H_2 evolution with TiO_2–Au NFs catalyst has been investigated.

Methods

Materials

Polyvinylpyrrolidone (PVP, $M_w \sim 1\,300\,000$) and chloroauric acid ($HAuCl_4 \cdot 3H_2O$, ≥99.9%) were purchased from Aldrich (St. Louis, MO, USA). Titanium isopropoxide (TTIP, $C_{12}H_{28}O_4Ti$, ≥99.9%), ethanol (EtOH) and acetic acid (HAc) were obtained from Chengdu Kelong Chemical Reagent Factory (Chengdu, China). All chemical reagents were analytically pure and used directly without further purification.

Fabrication of TiO_2–Au composite NFs with different gold content

TiO_2–Au composite NFs catalysts were synthesized through electrospinning (ES) combined with subsequent calcination process as shown in the schematic diagram (Fig. 1). In a typical process, PVP were dissolved in EtOH to obtain 7 wt% PVP–EtOH polymer solution, and then 1.5 g of TTIP were added into a mixture of 3 mL HAc and 3 mL EtOH, mixing with 6.43 g of the previous PVP–EtOH solution to form PVP–TTIP ES solution.[33] A given amount of gold precursor ($HAuCl_4 \cdot 3H_2O$) were added directly into the PVP–TTIP solution under vigorous stirring to form PVP–TTIP–Au ES solution and the mass ratio of Au/TiO_2 in the final products were 0 wt%, 3 wt%, 6 wt%, 9 wt%, and 12 wt%, respectively. The as-spun precursor NFs were obtained after a typical ES process, and then calcined at 500 °C for 2 hours in air to get the final products of TiO_2 NFs and TiO_2–Au composite NFs with different gold content, which were denoted as TiO_2–Au-0 wt% (equaled to bare TiO_2 NFs), TiO_2–Au-3 wt%, TiO_2–Au-6 wt%, TiO_2–Au-9 wt%, and TiO_2–Au-12 wt%, respectively. The commercial titania catalyst of Degussa P25 is chosen as the benchmark.

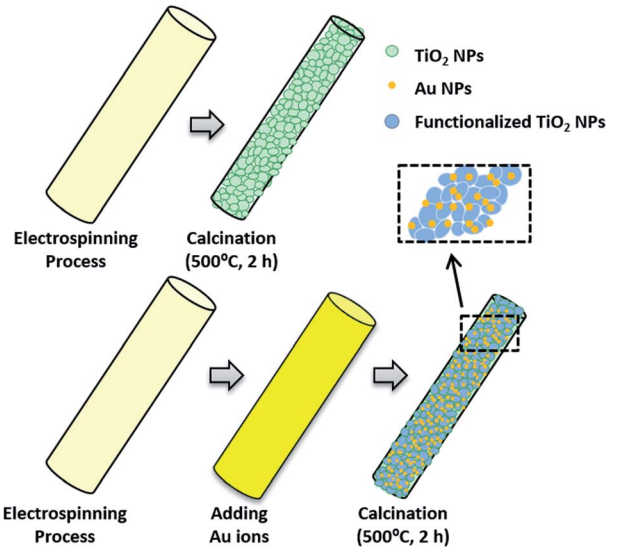

Fig. 1 Schematic diagram illustrating the formation of TiO_2–Au composite NFs.

Photocatalyst characterization

The morphologies and structures of the TiO_2–Au composite NFs were characterized by scanning electron microscope (SEM, Inspect F50, FEI, USA) and X-ray diffractometer (XRD, DX-2000, HAOYUAN, China), using Cu Kα1 $\lambda = 1.54056$ Å radiation. The average fiber diameter and particle size of samples were determined with software of Nano Measurer performed on SEM images. Transmission electron microscope (TEM) and high-resolution transmission electron microscope (HR-TEM) images, as well as energy-dispersive X-ray spectra (EDS) were obtained on a JEOL 2100F microscope to evaluate sample morphology and further confirm crystalline structures and elemental compositions. Photoluminescence (PL) spectra were performed with an excitation wavelength of 320 nm by a spectrofluorometer (FluoroMax-4, Horiba, Japan). UV-visible diffuse reflectance spectra (UV-vis) were obtained on a Shimadzu UV 3600 spectrophotometer.

Photocatalytic activity evaluation

The photocatalytic H_2 generation performances of all the samples were evaluated under full spectrum irradiation (a 300 W xenon arc lamp) for 3 hours. In a typical procedure, 30 mg of each prepared catalysts was dispersed in 150 mL of water/methanol mixture with the volume ratio of 9 : 1 under ultrasonic. In order to avoid the influence of air, argon was purged into the system half an hour to remove the air. And then the as-prepared suspension solution was irradiated under light (xenon lamp, 300 W) with magnetic stirring, and a water jacket was used to remove the thermal catalytic effect. The irradiation intensity for photocatalytic experiment was 380 mW cm^{-2}. During the photocatalytic H_2 generation process, the evolved gas was analyzed by using a gas chromatography (GC, 8A, Shimadzu) with an interval of 30 min.[34] Apparent quantum yield (AQY) of H_2 evolution were determined by using the equation of AQY (%) = (number of reacted electrons/number of incident photons) × 100%.[35]

Results and discussion

Gold content effects on morphologies and structures

The morphologies of TiO_2 NFs and TiO_2–Au composite NFs with different gold content were investigated by SEM as shown in Fig. 2. It can be seen that the TiO_2 NFs (average diameter of 160 nm) possess a rough surface while the TiO_2–Au composite NFs still have fibrous morphology, but with well dispersed bright dots, that were identified as gold NPs by XRD and TEM results. The gold NPs disperse homogeneous in all the TiO_2–Au composite NFs with different gold content. In order to check the effects of gold content on the particle size, the average size of gold nanoparticles for each sample were determined from measurements of SEM images performed on 100 particles using the software Nano Measurer. The gold nanoparticles can be divided in two types: one is uniform gold particles, another is

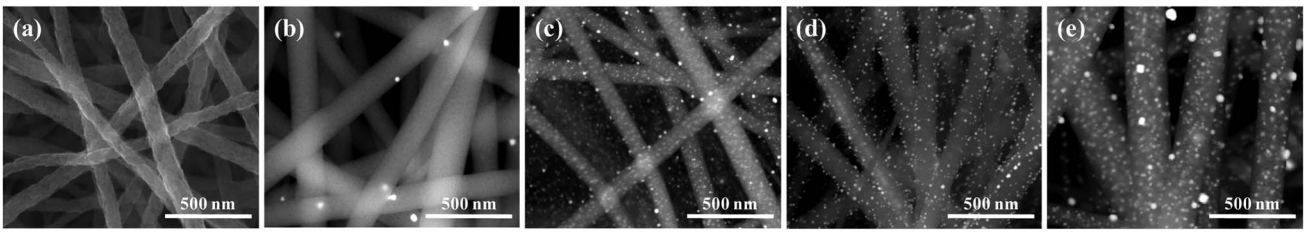

Fig. 2 SEM images of TiO_2–Au composite NFs with different gold content calcined at 500 °C in air for 2 h: (a) 0 wt%; (b) 3 wt%; (c) 6 wt%; (d) 9 wt% and (e) 12 wt%.

the nonuniform gold nanoparticles on the surface of TiO_2 fiber. Firstly, by analyzing the SEM images carefully, it can be seen that the gold nanoparticles with uniform size were of ~10 nm, which is contributed to the crystal of TiO_2 that preventing the growth of gold. And this comments also are confirmed by the related TEM images as shown in Fig. 4.

Secondly, the gold nanoparticles with nonuniform size and disturbing by the gold contents on the surface of TiO_2 NFs. The nanoparticles are more easily to migrate and aggregate to form larger nanoparticles with increasing of the gold content, that can overcome the inhibition from TiO_2 crystals. So the higher gold content the larger particle size should make sense in logical. However, the size of particle on the surface didn't have the direct relationship with gold content, it was random form tens of nanometer. The seed formation and particle growth are complicated and influenced by many factors of thermodynamics and kinetics, especially during the calcination process. Thus the size of gold nanoparticle on the surface of TiO_2–Au NFs with different contents were nonuniform. As increasing the gold content, the number of gold NPs increase, and the gold content in the final product can be varied precisely by the amount of gold precursor added in the ES solution.

It has been figured out by Wang *et al.*[34] that the intensity of the diffraction peaks of gold grows as increasing the gold content. Thus the sample with highest gold content of 12 wt% has been chosen and analyzed to check the difference between TiO_2 NFs and TiO_2–Au composite NFs more clearly. The crystal structures of P25, pure TiO_2 NFs and TiO_2–Au composite NFs (with gold content of 12 wt%) were determined by XRD as shown in Fig. 3. The XRD patterns of P25 and TiO_2 can be well-indexed to anatase (JCPDS card no. 00-021-1272). To check carefully, there are three others peaks for P25 could be found at $2\theta = 27.4°$, 36.1°, and 41.2° indexed as the (110), (101), and (111) planes of rutile (JCPDS card no. 00-021-1276), respectively.[32] Comparing to pure TiO_2, the XRD patterns of TiO_2–Au composite NFs are also well-indexed to anatase and there is no peaks related to rutile phase. Meanwhile, there are three additional peaks located at $2\theta = 44.4°$, 64.6°, and 77.5°, that correspond to the (200), (220), and (311) planes of the gold cubic phase (JCPDS card no.00-004-0784).[32] The commercial Titania Degussa P25 is the composite of anatase and rutile, while the sample of TiO_2 NFs and TiO_2–Au composite NFs are mainly of anatase. These results confirm that the TiO_2–Au composite NFs are composed of anatase and gold, and the crystal sizes were determined to be 20 nm and 8 nm based on the XRD patterns by using Scherrer's equation.

From TEM images (Fig. 4a), it can be seen that the NFs is well decorated with spherical NPs, where the average size is ~10 nm. The crystallographic (111) plane of gold and (101) plane of anatase are observed clearly with the corresponding lattice distance of 2.2 Å and 3.3 Å in the HRTEM images shown in Fig. 4b. Hence, the HRTEM results of TiO_2–Au composite NFs confirm that the gold NPs are well dispersed into TiO_2 NFs matrix, which is in accordance with the XRD results. Furthermore, the added elemental composition of gold and titanium (during the preparation of the photocatalysts) were matching with the composition of elements analyzed by EDS shown in Fig. 4c. Murdoch *et al.*[36] have reported that gold NPs with the size range of 3–30 nm deposited on TiO_2 are highly active, whereas there is no influence on the H_2 generation rate over the 3–12 nm range. Moreover, gold NPs with similar size has better functionalization effect on anatase than rutile NPs. Thus, the TiO_2–Au composite NFs with gold NPs (~10 nm) and anatase matrix of TiO_2 NFs are supposed to show good photocatalytic performance for H_2 evolution.

Gold content effects on optical properties

Photoluminescence (PL) measurement was conducted on all the samples with an excitation wavelength of 320 nm, to evaluate

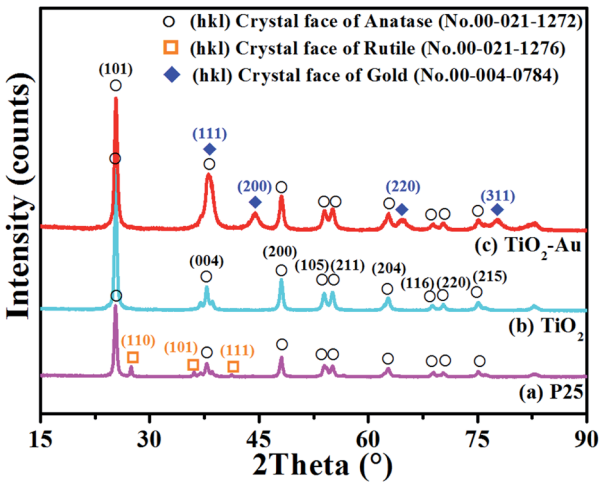

Fig. 3 XRD patterns of P25, TiO_2 NFs and TiO_2–Au-12 wt% composite NFs.

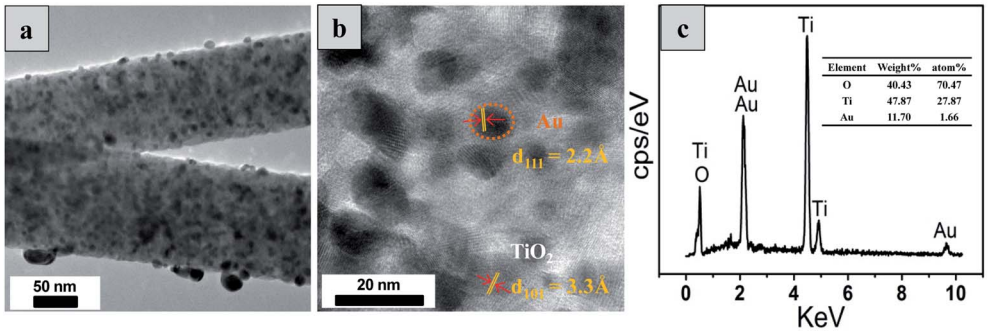

Fig. 4 (a) TEM image of TiO_2–Au-12 wt% composite NFs; (b) high-resolution TEM image of Au NPs embedded TiO_2 NFs showing the Au and TiO_2 lattices; (c) EDS spectrum of TiO_2–Au-12 wt% composite NFs.

the effects of gold content on the photoinduced charge transfer and charge recombination loss.[37] As shown in Fig. 5, the PL spectra of each sample have three main emission peaks located at 394 nm, 413 nm and 467 nm within a board emission band ranging from 375 nm to 500 nm. Comparing the PL intensity of all the samples, P25 possesses the highest intensity which is followed by TiO_2. After doping with gold NPs, the PL intensity of TiO_2–Au is lower than TiO_2, and the intensity gradually decreases as the gold content increasing. Au as an electron acceptor had a quantitative effect on the mediation of interfacial charge transfer. When the Au content increased, the emission lifetime was reduced, suggesting the significant decrease in the charge carrier separation at the interface.[38] It is reported that a higher PL peak intensity corresponds to a higher incidence of photogenerated carriers recombination within titanium powders.[39] The lower PL intensity for TiO_2–Au samples is attributed to the electrons transfer from TiO_2 conduction band to gold NPs; in this case the electron–hole recombination is restricted. Thus the photoexcited electrons are confined within gold NPs while holes remain at the TiO_2 valence band.[40] Consequently, TiO_2–Au composite NFs catalyst can significantly inhibit the recombination of photogenerated charge carriers.

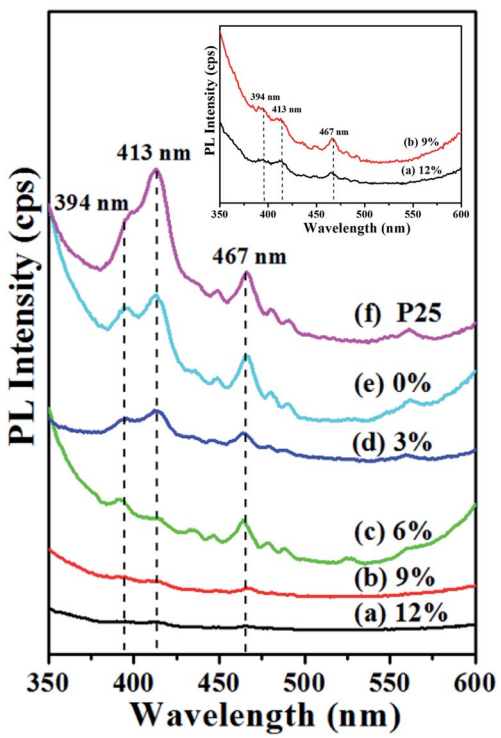

Fig. 5 Photoluminescence spectra of P25, TiO_2 NFs, and TiO_2–Au composite NFs with different gold content.

The UV-vis absorption spectra of all the samples are shown in Fig. 6. Comparing with the pure TiO_2 NFs and P25 that can only absorb UV light, the TiO_2–Au composite NFs have significant light absorption in the visible region (~380–780 nm) due to the surface plasmon resonance (SPR) effect of gold. In general, the semiconductor band gap is related to the light absorption capability where a decreased band gap indicates the increasing of absorption edge.[41] The absorbance curve of TiO_2–Au composite NFs exhibited an absorption edge red shift from ultraviolet to visible region compared with that of TiO_2 NFs. As increasing the gold content, the intensity of the SPR absorption peak in the visible region is dramatically increased, while the position of the SPR absorption peak shifted non-monotonically. The position and intensity of SPR absorbance peak are strongly depended on multiple factors, such as environment dielectric properties, the particle size, shape, size distribution and contents of gold NPs.[42] The gold NPs of TiO_2–Au composite NFs with different contents have different average size and distribution that was discussed in detail at the SEM parts. This could be the possible explanation for the non-monotonically shift.

As shown in Fig. 6b, the Tauc plots based on the UV-vis curves determine the band gaps, that are 3.15 eV and 2.75 eV for TiO_2 NFs and TiO_2–Au composite NFs, respectively.[43,44] The reduced band gap of TiO_2–Au composite NFs suggests that the presence of gold NPs can effectively increase the absorption edge and enhance the photocatalytic efficiency. It is also beneficial for extending the light absorption to the visible light range, that is one of the vital factors to improve the photocatalytic H_2 generation performance.[45] Therefore, TiO_2–Au composite NFs photocatalyst can be excited by visible light, resulting in an enhancement of H_2 generation.

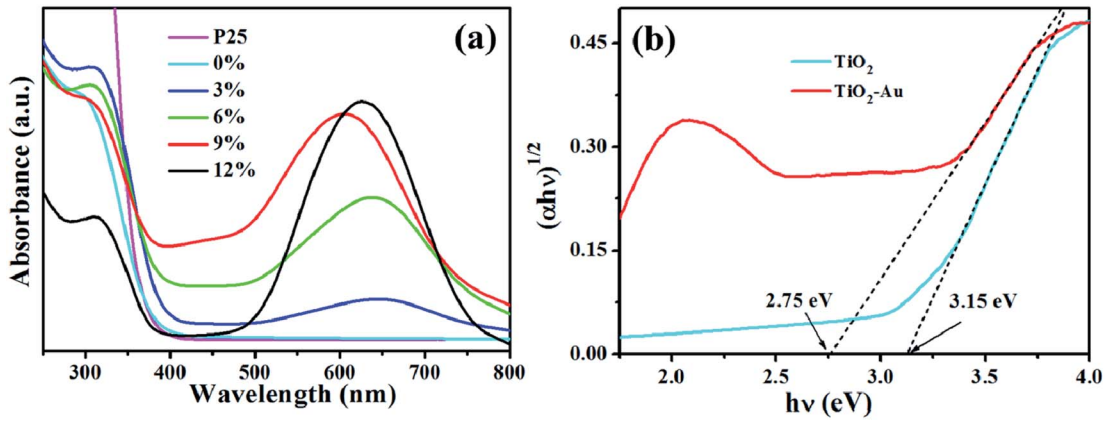

Fig. 6 UV-visible absorption spectra of (a) P25, pure TiO_2 and TiO_2–Au composite with different gold content; (b) Tauc plots of TiO_2 and TiO_2–Au-9 wt%.

Gold content effects on photocatalytic H_2 evolution

The H_2 evolution activity was compared among the P25, TiO_2 NFs, TiO_2–Au composites NFs with different gold content, and the H_2 evolution rate is compared by normalized as per gram of catalyst and per hour of irradiation time (as shown in Fig. 7). The linear increase of all the samples in the evolved H_2 indicates the stability of the catalyst. The lowest H_2 evolution activity of 584 μmol g^{-1} h^{-1} was obtained from commercial P25 with the specific surface area of 53.2 m^2 g^{-1}, while the activity increases more than 2 times of TiO_2 NFs (1254 μmol g^{-1} h^{-1}) with the specific surface area of 18.7 m^2 g^{-1}. The photocatalytic efficiency were promoted for TiO_2–Au composite NFs, attributing to the excitation of surface plasmon band by Au NPs. The excess of Au NPs loading on TiO_2 can enhance the local electromagnetic field and generate high-energy hot electrons.[46] As the gold content increasing from 3 wt% to 6 wt%, while the specific surface area decreased from 11.9 m^2 g^{-1} to 9.5 m^2 g^{-1}, leading to a higher H_2 generation. The TiO_2–Au composite NFs with the gold content of 9 wt%, showing a specific surface area of 8.4 m^2 g^{-1}, possesses the best photocatalytic performance of 12 440 μmol g^{-1} h^{-1}, which is almost 21 times higher than P25 and nearly 10 times of TiO_2. However, further increase of the gold content to 12 wt% resulted in the H_2 production of 1605 μmol g^{-1} h^{-1}, which is comparable with TiO_2–Au-3 wt% (1602 μmol g^{-1} h^{-1}). Au with relatively high content may function as recombination centers to invoke interfacial charge recombination instead of promoting charge separation.[46]

In order to exclude the contribution of specific surface area, the H_2 evolution rate was normalized for each sample. As shown in Table 1, the specific surface areas were decreased from 18.7 m^2 g^{-1} to 7.2 m^2 g^{-1}, as the gold contents increased from 0 wt% to 12 wt%. It had the same results that TiO_2–Au-9 wt% was the optimal sample of 1481 μmol h^{-1} m^{-2}, which was 135 times higher than P25 (11 μmol h^{-1} m^{-2}) and 22 times better than TiO_2 (67 μmol h^{-1} m^{-2}). It indicates that gold content is the predominant factor rather than the specific surface area for the photocatalytic efficiency. Meanwhile, the apparent quantum yield (AQY) of H_2 evolution for all the catalysts have been determined and provided in Table 1. The highest hydrogen generation rate of 12 440 μmol g^{-1} h^{-1}, corresponding to the AQY of 5.11% at 400 nm, is achieved for TiO_2–Au composite NFs with the gold content of 9 wt%. And the AQY are 0.24%, 0.52%, 0.66%, 1.19%, and 0.66% for P25, 0%, 3%, 6%, and 12%, respectively. When Au NPs with a suitable amount (9 wt%) were loading on TiO_2, the interfacial charge transfer of NFs was

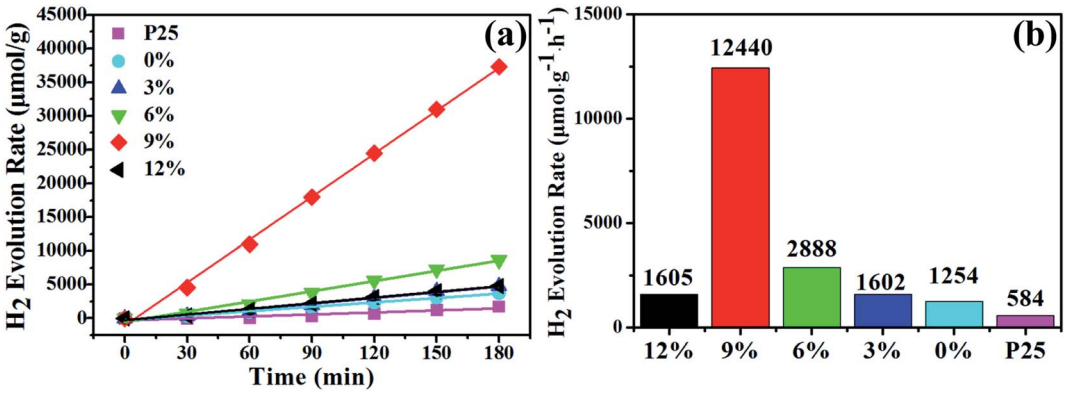

Fig. 7 H_2 evolution of P25, TiO_2 NFs and TiO_2–Au composite NFs catalyst with different gold content under light irradiation.

Table 1 H_2 evolution rate, apparent quantum yield at 400 nm, specific surface area and H_2 evolution rate normalized with specific surface area of each sample

Sample	P25	0%	3%	6%	9%	12%
H_2 evolution rate/μmol g^{-1} h^{-1}	584	1254	1602	2888	12 440	1605
Apparent quantum yield at 400 nm	0.24%	0.52%	0.66%	1.19%	5.11%	0.66%
Specific surface area/m^2 g^{-1}	53.2	18.7	11.9	9.5	8.4	7.2
H_2 evolution rate normalized with specific surface area/μmol h^{-1} m^{-2}	11	67	135	304	1481	223

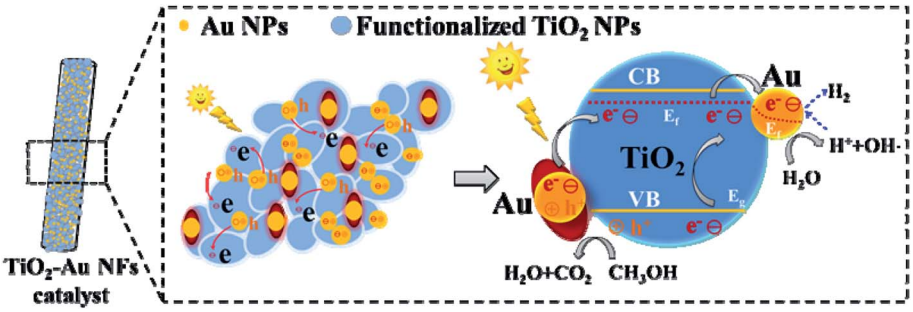

Fig. 8 Scheme of the photocatalytic H_2 generation mechanism of TiO_2–Au composite NFs.

highly mediated to render the facilitated electron scavenging from TiO_2, giving rise to an increased amount of photoexcited free electrons that could be extracted for further utilization.[47] These results indicate that the doping of gold NPs plays a positive role in increasing the H_2 generation efficiency, and the photocatalytic performance also has direct relation with the gold content.

Photocatalytic mechanism

The possible photocatalytic H_2 generation mechanism of TiO_2–Au composite NFs from water/methanol under light irradiation is proposed (Fig. 8). The TiO_2–Au composite NFs catalyst is photoexcited under light irradiation to generate the electron–hole pairs. The excited electrons from the valence band are transferred to conduction band, and then be more easily immigrate to the gold NPs band, due to the positive potential of gold compared with the conduction band level of TiO_2. Thus, the gold NPs act as efficient sinks for the excited electrons, whereby it can prolong the lifetime of the charge carriers.[19] Meanwhile, the gold NPs can also generate hot electrons owing to the surface plasmon resonance effect.[32] The hot electrons can be transferred to the adjacent TiO_2, greatly enhancing the potential light-harvesting capabilities of photocatalytic devices. Ratchford has been reported that the electron-injection efficiency from Au NPs to the TiO_2 ranges from about 25% to 45%, and the hot electrons spatial distribution is affected by the plasmonic field, with a higher generation rate for stronger electric field intensities.[48] Due to electromagnetic wave is transverse wave, the mostly incident light propagating approximately along the interface normal that are absorbed, so the optical electric field will be almost parallel to the interface. The relative weak light absorption efficiency and near field enhancement may be not beneficial to generation of a large number of hot electrons.[49] Thus the content of gold should have an optimal value. The adsorbed H_2O molecules react with the electrons on gold NPs to form the hydroxyl radicals ($OH^{\cdot}$) and hydrogen ion (H^+), and then the hydrogen ions (H^+) are reduced and converted into hydrogen molecules (H_2) by the photogenerated electrons trapped on the gold NPs. Meanwhile, the methanol (CH_3OH) molecular as hole scavenger, react with the holes left on the valence band of TiO_2 and to be further oxidized to CO_2 and H_2O.[34] The gold NPs play two roles during the photocatalytic H_2 evolution process, one is to enhance the light harvesting of TiO_2–Au composite materials from UV region to visible region and generate more charge carriers under light irradiation by surface plasmon resonance effect, and another one is to work as the electron sink to reduce the recombination rate of electron–hole pairs. This proposed mechanism demonstrates that the TiO_2–Au composite NFs catalyst can enhance the photocatalytic performance for H_2 production.

Conclusions

In summary, TiO_2–Au composite NFs were successfully fabricated by electrospinning combined with subsequent calcination. Gold NPs with uniform size (~10 nm) have been dispersed homogenously in TiO_2 NFs matrix (with average fiber diameter of 160 nm). The TiO_2–Au composite NFs photocatalyst showed excellent photocatalytic H_2 generation from a water/methanol mixture under light irradiation. The H_2 production rate of the TiO_2–Au composite NFs catalyst with the gold content of 9 wt% was dramatically enhanced to 12 440 μmol g^{-1} h^{-1}, corresponding to an adequate apparent quantum yield of 5.11% at 400 nm, which is 21 times and 10 times higher than that of P25 (584 μmol g^{-1} h^{-1}) and TiO_2 NFs (1254 μmol g^{-1} h^{-1}),

respectively. These results illustrate that gold NPs can facilitate the generation and transfer of photoinduced electron–hole pairs and play a vital role in boosting the H_2 production efficiency, which could be achieved by tuning the gold content to an optimal value. Furthermore, such TiO_2–Au composite NFs catalysts have significant potential for photocatalytic H_2 evolution and also provide a new strategy in solar energy conversion.

Conflicts of interest

There are no conflicts to declare.

Acknowledgements

This work has been financed by National Natural Science Foundation of China (Grant No. 51702224), the program of Sichuan Province Science and Technology Project (Grant No. 2017GZ0416) and the program of Postdoctoral Science Foundation of Sichuan University (Grant No. 2018SCU12001).

References

1 M. Zhao, H. Xu, S. Ouyang and H. Tong, Fabricating a Au@TiO_2 plasmonic system to elucidate alkali-induced enhancement of photocatalytic H_2 evolution: surface potential shift or methanol oxidation acceleration?, *ACS Catal.*, 2018, **8**(5), 4266–4277.

2 A. Fujishima, X. Zhang and D. Tryk, TiO_2 photocatalysis and related surface phenomena, *Surf. Sci. Rep.*, 2008, **63**(12), 515–582.

3 X. Chen, S. Shen, L. Guo and S. Mao, Semiconductor-based photocatalytic hydrogen generation, *Chem. Rev.*, 2010, **110**, 6503–6570.

4 E. Photocell, A. Fujishima and K. Kohayakawa, Hydrogen production under sunlight with an electrochemical photocell, *J. Electrochem. Soc.*, 1975, **122**(11), 1487–1489.

5 M. Altomare, N. Nguyen, S. Hejazi and P. Schmuki, A cocatalytic electron-transfer cascade site-selectively placed on TiO_2 nanotubes yields enhanced photocatalytic H_2 evolution, *Adv. Funct. Mater.*, 2018, **28**(2), 1–9.

6 J. Xu, W. Yang, S. Huang and H. Yin, CdS core-Au plasmonic satellites nanostructure enhanced photocatalytic hydrogen evolution reaction, *Nano Energy*, 2018, **49**, 363–371.

7 X. Lu, G. Wang, S. Xie and J. Shi, Efficient photocatalytic hydrogen evolution over hydrogenated ZnO nanorod arrays, *Chem. Commun.*, 2012, **48**, 7717–7719.

8 Z. Li, J. Liu, D. Wang and Y. Gao, Cu_2O/Cu/TiO_2 nanotube ohmic heterojunction arrays with enhanced photocatalytic hydrogen production activity, *Int. J. Hydrogen Energy*, 2012, **37**(8), 6431–6437.

9 F. Pellegrino, F. Sordello, M. Minella and C. Minero, The role of surface texture on the photocatalytic H_2 production on TiO_2, *Catalysts*, 2019, **9**(32), 1–28.

10 A. S. Hainer, J. S. Hodgins, V. Sandre and M. Vallieres, Photocatalytic hydrogen generation using metal-decorated TiO_2: sacrificial donors *vs.* true water splitting, *ACS Energy Lett.*, 2018, **3**(3), 542–545.

11 Y. Yang, K. Ye, D. Cao and P. Gao, Efficient charge separation from f-selective etching and doping of anatase–TiO_2{001} for enhanced photocatalytic hydrogen production, *ACS Appl. Mater. Interfaces*, 2018, **10**(23), 19633–19638.

12 R. Su, R. Tiruvalam, A. J. Logsdail and Q. He, Designer titania-supported Au–Pd nanoparticles for efficient photocatalytic hydrogen production, *ACS Nano*, 2014, **8**(4), 3490–3497.

13 X. An, C. Hu, H. Liu and J. Qu, Hierarchical nanotubular anatase/rutile/TiO_2(B) heterophase junction with oxygen vacancies for enhanced photocatalytic H_2 production, *Langmuir*, 2018, **34**(5), 1883–1889.

14 Y. H. Chiu, T. H. Lai, C. Y. Chen and P. Y. Hsieh, Fully depleted Ti–Nb–Ta–Zr–O nanotubes: interfacial charge dynamics and solar hydrogen production, *ACS Appl. Mater. Interfaces*, 2018, **10**(27), 22997–23008.

15 P. Y. Hsieh, Y. H. Chiu, T. H. Lai and M. J. Fang, TiO_2 nanowire-supported sulfide hybrid photocatalysts for durable solar hydrogen production, *ACS Appl. Mater. Interfaces*, 2019, **11**(3), 3006–3015.

16 J. M. Li, C. W. Tsao, M. J. Fang and C. C. Chen, TiO_2–Au–Cu_2O photocathodes: Au-mediated *Z*-scheme charge transfer for efficient solar-driven photoelectrochemical reduction, *ACS Appl. Nano Mater.*, 2018, **1**(12), 6843–6853.

17 Y. S. Chang, M. Choi, M. Baek and P. Y. Hsieh, CdS/CdSe co-sensitized brookite H:TiO_2 nanostructures: charge carrier dynamics and photoelectrochemical hydrogen generation, *Appl. Catal., B*, 2018, **225**, 379–385.

18 A. Tanaka, S. Sakaguchi, K. Hashimoto and H. Kominami, Preparation of Au/TiO_2 with metal cocatalysts exhibiting strong surface plasmon resonance effective for photoinduced hydrogen formation under irradiation of visible light, *ACS Catal.*, 2013, **3**(1), 79–85.

19 C. Marchal, T. Cottineau, M. G. Méndez-Medrano and C. Colbeau-Justin, Au/TiO_2–gC_3N_4 nanocomposites for enhanced photocatalytic H_2 production from water under visible light irradiation with very low quantities of sacrificial agents, *Adv. Energy Mater.*, 2018, **8**, 702142.

20 Y. H. Chiu, K. D. Chang and Y. J. Hsu, Plasmon-mediated charge dynamics and photoactivity enhancement for Au-decorated ZnO nanocrystals, *J. Mater. Chem. A*, 2018, **6**(10), 4286–4296.

21 K. H. Chen, Y. C. Pu, K. D. Chang and Y. F. Liang, Ag-nanoparticle-decorated SiO_2 nanospheres exhibiting remarkable plasmon-mediated photocatalytic properties, *J. Phys. Chem. C*, 2012, **116**(35), 19039–19045.

22 X. Liu, H. Lai, J. Li and G. Peng, Polyaniline sensitized Pt@TiO_2 for visible-light-driven H_2 generation, *Int. J. Hydrogen Energy*, 2018, **44**(10), 4698–4706.

23 J. He, M. Wang, X. Wu and Y. Sun, Influence of controlled Pd nanoparticles decorated TiO_2 nanowire arrays for efficient photoelectrochemical water splitting, *J. Alloys Compd.*, 2019, **785**, 391–397.

24 F. Xue, C. Chen, W. Fu and M. Liu, Interfacial and dimensional effects of Pd co-catalyst for efficient photocatalytic hydrogen generation, *J. Phys. Chem. C*, 2018, **122**, 25165–25173.

25 M. J. Li, H. Y. Cheng, Y. H. Chiu and Y. J. Hsu, ZnO–Au–SnO_2 *Z*-scheme photoanodes for remarkable photoelectrochemical water splitting, *Nanoscale*, 2016, **8**(34), 15720–15729.

26 Z. W. Seh, S. Liu, M. Low and S. Zhang, Janus Au–TiO_2 photocatalysts with strong localization of plasmonic near-fields for efficient visible-light hydrogen generation, *Adv. Mater.*, 2012, **24**, 2310–2314.

27 Y. C. Pu, G. M. Wang, K. D. Chang and Y. C. Ling, Au nanostructure-decorated TiO_2 nanowires exhibiting photoactivity across entire UV-visible region for photoelectrochemical water splitting, *Nano Lett.*, 2013, **13**(8), 3817–3823.

28 M. Ge, J. Cai, J. Iocozzia and C. Cao, A review of TiO_2 nanostructured catalysts for sustainable H_2 generation, *Int. J. Hydrogen Energy*, 2016, **42**(12), 8418–8449.

29 S. Chuangchote, J. Jitputti, T. Sagawa and S. Yoshikawa, Photocatalytic activity for hydrogen evolution of electrospun TiO_2 nanofibers, *ACS Appl. Mater. Interfaces*, 2009, **1**(5), 1140–1143.

30 D. Li and Y. Xia, Electrospinning of nanofibers: reinventing the wheel?, *Adv. Mater.*, 2004, **16**(14), 1151–1170.

31 D. Li, J. T. McCann, M. Gratt and Y. Xia, Photocatalytic deposition of gold nanoparticles on electrospun nanofibers of titania, *Chem. Phys. Lett.*, 2004, **394**, 387–391.

32 X. Yang, Synthesis and characterization of hybrid metal–metallic oxide composite nanofibers by electrospinning and their applications, Materials and structures in mechanics [physics.class-ph], PhD thesis, Université de Lyon, 2016.

33 D. Li and Y. Xia, Fabrication of Titania Nanofibers by Electrospinning, *Nano Lett.*, 2003, **3**(4), 555–560.

34 F. Wang, Y. Jiang, A. Gautam and Y. Li, Exploring the origin of enhanced activity and reaction pathway for photocatalytic H_2 production on Au/B–TiO_2 catalysts, *ACS Catal.*, 2014, **4**, 1451–1457.

35 Y. H. Chiu, S. B. Naghadeh, S. A. Lindley and T. H. Lai, Yolk-shell nanostructures as an emerging photocatalyst paradigm for solar hydrogen generation, *Nano Energy*, 2019, **62**, 289–298.

36 M. Murdoch, G. I. N. Waterhouse, M. A. Nadeem and J. B. Metson, The effect of gold loading and particle size on photocatalytic hydrogen production from ethanol over Au/TiO_2 nanoparticles, *Nat. Chem.*, 2011, **3**(6), 489–492.

37 X. Wang, H. Wang, H. Zhang and W. Yu, Dynamic interaction between methylammonium lead iodide and TiO_2 nanocrystals leads to enhanced photocatalytic H_2 evolution from HI splitting, *ACS Energy Lett.*, 2018, **3**, 1159–1164.

38 Y. H. Hsu, A. T. Nguyen, Y. H. Chiu and M. J. Li, Au-decorated GaOOH nanorods enhanced the performance of direct methanol fuel cells under light illumination, *Appl. Catal., B*, 2016, **185**, 133–140.

39 L. Kernazhitsky, V. Shymanovska, T. Gavrilko and V. Naumov, Room temperature photoluminescence of anatase and rutile TiO_2 powders, *J. Lumin.*, 2014, **146**, 199–204.

40 W. H. Saputera, J. Scott, N. Ganda and G. K. C. Low, The role of adsorbed oxygen in formic acid oxidation by Pt/TiO_2 facilitated by light pre-treatment, *Catal. Sci. Technol.*, 2016, **6**(17), 6679–6687.

41 Q. Wang, N. An, Y. Bai and H. Hang, High photocatalytic hydrogen production from methanol aqueous solution using the photocatalysts CuS/TiO_2, *Int. J. Hydrogen Energy*, 2013, **38**(25), 10739–10745.

42 T. Hendel, M. Wuithschick, F. Kettemann and A. Birnbaum, *In situ* determination of colloidal gold concentrations with UV-vis spectroscopy: limitations and perspectives, *Anal. Chem.*, 2014, **86**, 11115–11124.

43 M. Aiempanakit, T. Tabtimsri, N. Triamnak and C. Suwanchawalit, Curcumin modified titanium dioxide nanotubes with enhanced visible light photocatalytic performance, *Int. J. Electrochem. Sci.*, 2019, **14**, 1954–1967.

44 A. A. Ismail and D. W. Bahnemann, Synthesis of TiO_2/Au nanocomposites *via* sol–gel process for photooxidation methanol, *J. Adv. Oxid. Technol.*, 2009, **12**(1), 9–15.

45 A. Madhumitha, V. Preethi and S. Kanmani, Photocatalytic hydrogen production using TiO_2 coated iron-oxide core shell particles, *Int. J. Hydrogen Energy*, 2018, **43**(8), 3946–3956.

46 W. H. Lin, Y. H. Chiu, P. W. Shao and Y. J. Hsu, Metal-particle-decorated ZnO nanocrystals: photocatalysis and charge dynamics, *ACS Appl. Mater. Interfaces*, 2016, **8**(48), 32754–32763.

47 Y. C. Chen, Y. C. Pu and Y. J. Hsu, Interfacial charge carrier dynamics of the three-component In_2O_3–TiO_2–Pt heterojunction system, *J. Phys. Chem. C*, 2012, **116**(4), 2967–2975.

48 D. C. Ratchford, A. D. Dunkelberger, I. Vurgaftman and J. C. Owrutsky, Quantification of efficient plasmonic hot-electron injection in gold nanoparticle-TiO_2 films, *Nano Lett.*, 2017, **17**(10), 6047–6055.

49 X. Ma, Y. Dai, L. Yu and B. Huang, New basic insights into the low hot electron injection efficiency of gold-nanoparticle-photosensitized titanium dioxide, *ACS Appl. Mater. Interfaces*, 2014, **6**, 12388–12394.

